Modeling Bidirectional Radiance Measurements Collected by the Advanced Solid-State Array Spectroradiometer (ASAS) over Oregon Transect Conifer Forests

*Abdelgadir A. Abuelgasim** and Alan H. Strahler**

A geometric-optical model of the bidirectional reflectance of a forest canopy, developed by Li and Strahler, fits observed directional radiance measurements with good accuracy. This model treats the forest cover as a scene of discrete, three-dimensional objects (trees) that are illuminated and viewed from different positions in the hemisphere. The shapes of the objects, their count densities and patterns of placement, are the driving variables, and they condition the mixture of sunlit and shaded objects and background that are observed from a particular viewing direction, given a direction of illumination. This mixture, in turn, controls the brightness apparent to an observer or a radiometric instrument. The Advanced Solid-State Array Spectroradiometer (ASAS) was used to validate this model. This aircraft sensor presently acquires images in 29 spectral bands in the range (465–871 nm) and is pointable fore-and-aft, allowing directional measurements of radiance as a target is approached and imaged at view angles ranging $\pm 45°$ from nadir. Through atmospheric correction, ASAS radiances were reduced to bidirectional reflectance factors (BRFs). These were compared to corresponding BRF values computed from the Li–Strahler model using, wherever possible, ground measured component BRFs for calibration. The comparisons showed a good match between the modeled and measured reflectance factors for four of the five Oregon Transect Sites. Thus, the geometric-optical approach provides a realistic model for the bidirectional reflectance distribution function of such natural vegetation canopies. Further modifications are suggested to improve the predicted BRFs and yield still better results.

INTRODUCTION

Remotely sensed data have been commonly used to obtain quantitative information on the biophysical characteristics of vegetation. These characteristics and their spatial and temporal distribution are critical inputs to ecological models that describe the interaction between land surface and climate, energy balance, and hydrologic and biochemical cycles. An important mechanism for the inference of biophysical information is the application of vegetation canopy reflectance models, ably reviewed in a recent book by Myneni and Ross (1991). The contributions of canopy reflectance modeling have been considerable, particularly in improving our understanding of the influence of vegetation parameters on reflectance of radiation (Myneni and Ross, 1991). Notable progress has been gained in the understanding of the total amount of reflected radiation, and its spectral and angular distribution (Suits, 1972a,b; Jackson et al., 1979; Cooper et al., 1982; Kimes, 1984; Otterman and Weiss, 1984, Li and Strahler, 1986, 1992a; Jupp and Strahler, 1991). Much effort has been devoted to understanding and remodeling the dependence of the bidirectional reflectance distribution function (BRDF) of vegetation-covered Earth surfaces as a function of various environmental, structural, and physiological conditions, as well as viewing and illumination geometries. Typical approaches have included two-stream, radiative transfer, geometric optics, hybrids of two or more of these, and numerical simulation. Some are applicable to continuous vegetation cover, such as crops, and others are best utilized for discontinuous covers, such as forests.

The earliest practical plant canopy reflectance model is that of Suits (1972a), which adds direct irradiation and directional existance to a two-stream Kubelka–Monk (1931) model. The hotspot is treated as an empirical function reducing the attenuation of exiting radiation as a function of the phase angle between illumination and view directions. The model assumes that leaves are Lambertian and either vertical or horizontal. It has been

*Center for Remote Sensing and Department of Geography, Boston University

Address correspondence to Dr. Alan Strahler, Center for Remote Sensing, Boston University, 725 Commonwealth Ave, Boston, MA 02215.

extended by Verhoef (1984) to the case of a variable leaf-angle distribution (the SAIL model) and by Reyna and Bhadwar (1985) to include a specular reflectance component. More recently, Jupp and Strahler (1991) have added a proper geometric–optical kernel to the Suits model that is driven by leaf shape, arrangement, and spacing.

In classical radiative transfer models, the medium is typically treated as a horizontally uniform series of plane-parallel layers composed of small absorbing and scattering particles. This type of model is well established for interaction between radiation and the atmosphere (Chandrasekhar, 1950), but in the case of a vegetation canopy, the scattering elements, that is, leaves, are of finite size, and thus a pure radiative transfer approach is not possible (Myneni et al., 1991). The shadowing behavior that produces the hotspot through enhanced single scattering must be accommodated for a radiative transfer model to be realistic. Sometimes this is included in an empirical angular dependence of irradiance to solar zenith angle for the canopy as a whole (Ross, 1981); in other treatments, the phase function of the leaf surface is separated from a phase function that describes the hotspot (Verstraete et al., 1990). The hotspot function can take several forms, sometimes fully empirical, other times driven by the shape, orientation, and / or spacing of the leaves. The functions include piecewise-linear, negative-exponential, geometric, and trigonometric. Examples may be found in the models developed by Kuusk (1985), Gerstl et al. (1986), Myneni et al. (1990), Myneni and Ross (1991), and Marshak (1989). Two-stream solutions have been driven by Nilson and Kuusk (1989) and Nilson and Peterson (1991). These types of models are best applied to continuous vegetation covers such crops or homogeneous grasslands.

In the geometric–optical approach, the bidirectional reflectance is modeled as a purely geometric phenomenon that results when scenes of discrete, three-dimensional objects are illuminated and viewed from different positions in the hemisphere. The shape of the objects, their count densities and patterns of placement are the driving variables, and they condition the mixture of sunlit and shaded objects and background that is observed from a particular view direction, given a certain direction of illumination (Li and Strahler, 1986). This mixture in turn controls the brightness apparent to an observer or a radiometric instrument. Li and Strahler (1985; 1986; 1992a) emphasized the individual tree canopy as the functional element in modeling, and have applied geometric–optical models of bidirectional reflectance successfully for open and moderately closed stands of conifers treated as "green" cones or spheroids on a contrasting background. Jupp et al. (1986) used a similar approach for trees as spheroidal objects, and

extended the treatment to two crown layers above a background using Boolean logic of Serra (1982). Recently, Strahler and Jupp (1990) have provided a more general Boolean treatment that includes leaves within discrete-crown envelopes as a two-stage nest model. An approach very similar to that of Li and Strahler was developed independently by Nilson (1977), and published in a technical report of the Estonian Academy of Science (in Russian). This report was unavailable in the West at that time, and it was not until the end of the 1980s that Nilson's work became known here.

Although the geometric–optical approach properly models the three-dimensional nature of the scene with due complexity, it greatly simplifies the interaction between elements due to multiple scattering among leaves and individual canopies. Li and Strahler (1986) modeled the reflectance associated with a given viewpoint as an area-weighted sum of four fixed reflectance components, namely, sunlit leaves or canopy, sunlit background, shaded leaf or canopy, and shaded background. Since the reflectance of a sunlit plant crown will be a function of canopy depth, which will be lesser near the edges of the crown and greater near the center, this signature will not be uniform. Also, the shaded canopy signature will not be uniform, as it is related to the radiation penetrating through the crown, the diffuse skylight distribution, and multiply scattered radiation from the ground and other crowns into the shaded portion. Due to similar effects, the signatures of sunlit and shaded canopy or leaf will also be heterogenous. However, if the variance in signatures within components is significantly less than that among component signatures, this assumption may not be a significant limitation.

Li and Strahler noted a further problem with their (1986) geometric–optical model when either or both illumination and viewing direction assumed large zenith angles. At such angles, the tops of the trees are more likely to be illuminated and visible than the shaded lower portions, and thus the scene will appear brighter than a model simply based on random shadowing would predict. This gives the BRDF a "bowl shape," in which the reflectance increases for a given sun angle as the observer descends to a position low on the horizon (Kimes et al., 1986). This effect was referred to as the mutual-shadowing problem, since it arises because of the mutual shadowing and obscuring of crowns by one another. A treatment for the mutual-shadowing problem was thus added to the earlier model (Li and Strahler, 1992a,b). The present version properly reflects the shadow interaction given the count density of the objects.

A primary objective of this research is to validate and test the mutual-shadowing geometric–optical model developed by Li and Strahler (1992a) against actual directional reflectance measurements collected by the

Advanced Solid-state Array Spectroradiometer (ASAS) (Irons et al., 1991). This airborne pushbroom scanner can be tilted fore and aft, and thus has the unique capability to collect measurements at different viewing angles. As part of a larger ecosystem study (the OTTER Project), conifer stands along a transect across west-central Oregon were imaged by ASAS (Peterson and Waring, 1993). Because the reflectance measurements were collected over forests across a large environmental gradient, different species canopy structures and varying densities were observed, allowing the model to be validated in canopies with different characteristics.

The general procedure was to compare the BRF shape and absolute reflectance as predicted by the model to that observed by the ASAS. This was carried out by running the model at the test sites using actual tree geometry measurements and component signatures measured with a spectral radiometer, yielding the model-calculated BRF. Processing the ASAS images to calculate mean radiances and bidirectional reflectance factors (BRFs) yielded the actual shape and absolute reflectance values of the BRFs of the test sites. Predicted model BRFs and the actual measured BRFs were then compared.

LI-STRAHLER GEOMETRIC-OPTICAL BRDF MODEL

The Li-Strahler model treats canopies as three-dimensional objects with fixed shape but varying size. The objects are randomly distributed on a contrasting background, and are illuminated at a given direction. A tree crown is taken as a simple geometric object, in this case a spheroid, centered at some distance above the ground. The form parameters that describe the shape of the spheroid relative to its height above the ground are known previously and are invariant, while tree size varies. The radiance of a pixel is an area-weighted sum of the radiance signature for four components, namely, sunlit crown, sunlit background, shaded crown, and shaded background. It is the size and density of the tree crowns that determine the proportions of these components within a pixel. That is,

$$R = K_g G + K_c C + K_t T + K_z Z,$$

where R is the brightness of a pixel, G, C, T, and Z are the spectral signatures of the respective components, and K_g, K_c, K_t, and K_z are the areal proportions of sunlit background, sunlit crown, shaded crown, and shaded background, respectively.

In Li and Strahler (1986), the BRDF of a pixel is modeled as the limit of its directional reflectance factor $R(i, v)$ when both the solid angles of incoming and outgoing directions go to zero:

$$R(i, v) = \int_A \frac{R(s)\langle i, v \rangle \langle v, s \rangle I_{i(s)} I_{v(s)} \, ds}{A \cos \theta_i \cos \theta_v}, \qquad (1)$$

where ds is a small Lambertian surface element over area A of a pixel; $R(s)$ is the reflectance of ds; i, v, and s represent the directions of illumination, viewing and the normal to a surface element, respectively; $\langle \cdots \rangle$ is the cosine of the phase angle between two directions; $I_{i(s)}$ and $I_{v(s)}$ are indicator functions, equal to 1 if ds is illuminated (I_i) or viewed (I_v), zero otherwise, and θ is the zenith angle of a direction.

To explain the analysis further, let us assume that there are only two kinds of surfaces over the pixel area A, namely background surface and crown surface with Lambertian reflectance G and C, respectively. A_g and A_c will denote the area of background that is both illuminated and viewed and the area of crown both illuminated and viewed, respectively; both are as projected into the sensor's footprint on the ground. Then $R(i, v)$ may be written as

$$R(i, v) = K_g G + \frac{C}{A} \int_{A_c} \frac{\langle i, s \rangle}{\cos \theta_i} \frac{\langle v, s \rangle}{\cos \theta_v} \, ds, \qquad (2)$$

where $K_g = A_g / A$ is the proportion of background both illuminated and viewed. Considering that the union of A_g and A_c is the intersection of the set of surface elements that are illuminated and the set of those that are viewed, only when v and i coincide can A_g and A_c achieve a maximum, provided that the surface elements have no spatial orientation preference. Thus, the hotspot is well explained by this equation. Another obvious and important meaning of this equation is that the directional reflectance of a scene depends not only on the material reflectance (related to G and C), but also on its spatial structure, which determines A_g and A_c.

It will be helpful to investigate the two terms of Eq. (2). The first term describes how the sunlit background proportion proceeds to a maximum as viewing and illumination coincide, and the second describes how the sunlit crown surface, composed of Lambertian facets, similarly becomes maximally exposed to view at the hotspot.

OVERLAP FUNCTION FOR CROWNS

To investigate how the first term in Eq. (2) varies with illumination and viewing geometry, the crowns are assumed to have the shape of a spheroid (Strahler and Jupp, 1990) with vertical half-axis equal to b, horizontal radius equal to R, and height to the center of the spheroid h. For accommodating the spheroidal shape easily in the derivations of the shadow areas that follow, a transformation will be used that simply replaces θ by the angle that would generate the same shadow area for a sphere; that is, $\theta' = \tan^{-1}(b \tan \theta / R)$. The symbol

λ will denote the density of spheroids, that is, $\lambda = n / A$, where n is the count of crown centers within the sensor's footprint A. Assuming that G and C are constant as average signatures over A_g and A_c, (2) will thus need to properly model K_g and $K_c = A_c / A$.

Using the Boolean model of Strahler and Jupp (1990), K_g in (2) can be expressed as

$$K_g = e^{-\lambda \pi R2[\sec \theta'_i + \sec \theta'_v - \overline{O}(\theta_i, \theta_v, \varphi)]}, \tag{3}$$

where $\overline{O}$ $(\theta_i, \theta_v, \varphi)$ is the average of the overlap function between illumination and viewing shadows of individual crowns as projected onto the background. Here φ is the difference in azimuth angle between viewing and illumination positions.

Strahler and Jupp (1990) approximated the overlap function by the overlap area of two disks with the original areas and center positions of the two ellipses. To improve the accuracy and preserve the proper hotspot width information, Li and Strahler developed another approximation better suited to case of ellipses intersecting at arbitrary angles (1992a).

CONTRIBUTION OF SUNLIT CANOPY SURFACE

The modeling of the effect of the sunlit canopy on the bidirectional reflectance [second term in (2)] is more difficult cause it depends on both the density and the angular distribution of ds in (2). Strahler and Jupp (1990) assumed that each crown could be modeled as a sphere without mutual illumination shading between ds elements. Thus, the second term can be approximated as

$$K_c C = 1 / 2(1 + \langle i, v \rangle)(1 - e^{-\lambda \pi R2 \sec \theta_v})C. \tag{4}$$

In this expression, the first term is the illuminated proportion of the area of a single sphere viewed at position v and illuminated at position i, which ranges from 1, at 0 phase angle, to 0, when both viewing and illumination are opposite and the phase angle is therefore π. This is weighted by the second term, which is the proportion of the area of spheres visible from zenith angle θ_v. Since both terms vary smoothly between 0 and 1, this contribution to the hotspot is quite flat; in the case of a spheroid, $\langle i, v \rangle$ can be replaced by $\langle i', v' \rangle$, where

$$\langle i', v' \rangle = \cos \theta'_i \cos \theta'_v + \sin \theta'_i \sin \theta'_v \cos \varphi. \tag{5}$$

The first term in (4) ignores the mutual shadowing of one canopy by another. That is, when either the view or illumination direction is near the horizon, viewing and / or illumination shadows will fall on the spheroids, thus shading or obscuring some of the facets. Li and Strahler (1992a) developed a simple approximation to describe the effect for vegetation covers composed of collections of individual, discrete canopies. Their approach applies one-stage geometric optics to deal with

the spatial relationship between the part of the crown surface that is mutually shaded in the illumination direction and the part mutually shaded in the view direction.

MUTUAL SHADOWING TREATMENT

In developing a mathematical formulation for the mutual shadowing index, let us consider the proportion of crown surface that will be mutually shadowed by other crowns. In the direction of illumination, each crown has an area $\pi R^2 \sec \theta'_i$ projected onto the ground, the total projected area (as a proportion of A) then will be $\lambda \pi R^2 \sec \theta'_i$, if there is no mutual shadowing. Because of the mutual shadowing, however, the net projected area will be $1 - e^{-\lambda \pi R2 \sec \theta'_i}$. The difference therefore will indicate the total mutual shadowing. Thus a quantity M_i can be defined as the mutual shadowing proportion in the illumination direction, as

$$M_i = 1 - \frac{1 - e^{-\lambda \pi R2 \sec \theta'_i}}{\lambda \pi R^2 \sec \theta'_i}. \tag{6}$$

M_i will therefore be an index showing the degree of mutual shadowing in the illumination direction. In other words, each spheroid will, on average, have a proportion that will not be sunlit, which will likely be in the lower part of the spheroid. This means that we may also take M_i to be a normalized shadow area, which we assume will occupy the lower part of the spheroid (see Fig. 1).

Figure 1. Diagram showing M_i and M_v for a spheroid.
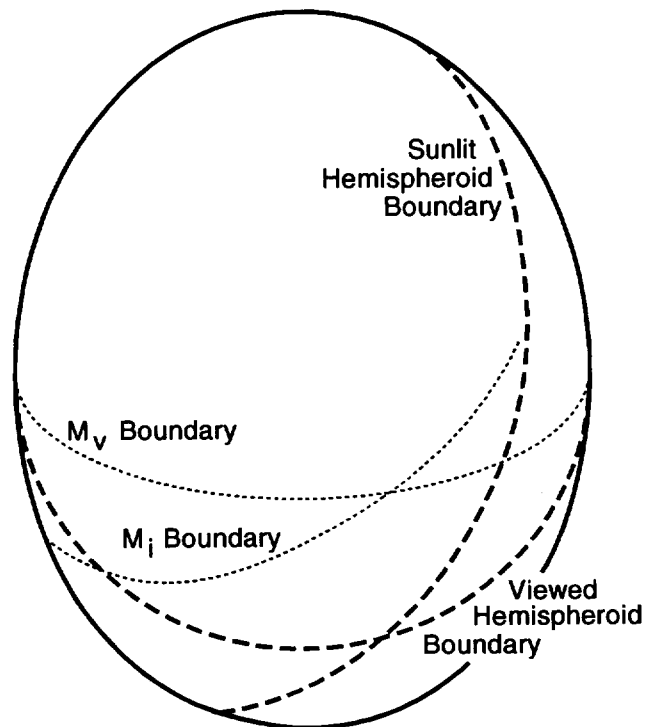
Similarly, the mutual shadowing proportion in the view direction can be defined as

$$M_v = 1 - \frac{1 - e^{-\lambda \pi R^2 \sec \theta_v}}{\lambda \pi R^2 \sec \theta_v}. \tag{7}$$

Clearly, the proportion of sunlit crown the sensor can see depends on both zenith and azimuth differences between the illumination and view directions. At the hotspot, M_i and M_v boundaries will overlap, and the sensor will see no mutual shadowing. When the view zenith angle is larger than the illumination zenith angle, M_v will be greater than M_i, and little or no mutually shaded crown will be visible. Thus, this simplification captures the essence of the mutual shadowing effect (Li and Strahler, 1992a). However, the true situation is that the mutual shadowing will not be strictly under the M_i or M_v boundaries unless the crown centers are uniformly located at the same height. This may be referred to as the "uniform" case. In contrast is the "random" case, where illumination and viewing shadows are independently scattered on other crowns, and thus the contribution of mutual shadowing to both the hot spot and bowl shape can be ignored. This obviously applies to the case where the crown centers are vertically well separated.

In general, the practical situation is always between these two extremes, depending upon the height distribution. If all crowns are at the same height, the situation will be very close to the "uniform height" case. The mutual shadows will always fall on the lower part of the crowns and get higher and higher when zenith angle increases, and thus the crown-top viewing effect will be strong. However, when tree heights are distributed over a wide vertical range, the top layer of the forest canopy will play a more important role in determining the BRDF of the canopy than lower layers. So, in general, when crown heights are distributed in a wide range, the bowl shape of the BRDF will be determined basically by size, shape, and height of crowns in the top layer. Thus, Li and Strahler (1992a) considered a single top layer only, and assumed that when the range of distribution of height approximately equals or exceeds twice the vertical axis of the spheroid, the random case dominates, whereas when the heights are uniform, the uniform case dominates. The empirical parameter β was used to describe the variation between these two extremes.

Since their 1992a article, Li and Strahler had derived a better formula for β, the mutual shadowing coefficient:

$$\beta = \frac{\lambda \Gamma_i}{\lambda \Gamma_i + (h_2 - h_1)/D} \frac{1 - e^{-\lambda \Gamma_i + (h_2 - h_1)/D}}{1 - e^{\lambda \Gamma_i}}, \tag{8}$$

where D is the decorrelation depth of a single crown at nadir viewing, defined as $D = R \cot(\theta_i/2)$. This equation is simple but includes almost all factors which determine the canopy structure and illumination geome-

try. The ratio $(h_2 - h_1)/D$ represents the thickness of canopy in units of correlation depth, and plays a role relating canopy structure and illumination geometry together.

From (8), it would be noted that for a given coverage and sun position $(\lambda \Gamma_i)$, β will decrease from 1 to 0 with increasing canopy depth from 0 to ∞; and for a given canopy depth, β increases from a value determined by canopy depth to 1 with increasing coverage from 0 to ∞.

Note that the mutual shadowing model generates a BRDF, whereas we are comparing that to a BRF. In the case of clear sky, the diffuse sky light is negligible compared to direct sun light in the red and near infrared wavelengths, and the measurement of the reference panel can be regarded as good indicator of direct solar irradiance. Furthermore, the component signatures used to calibrate the mutual shadowing model are influenced by any diffuse irradiance that may exist, as well as mutual scattering. Thus, the modeled BRDF should approximate a BRF in this situation.

FIELD SITES AND DATA COLLECTION

Test Sites

This research was carried out as part of the overall OTTER project. The main objective of the Oregon Transect Ecosystem Research Project (OTTER) was to test and validate an ecosystem process model, FOREST-BGC, across a broad range of coniferous forest ecosystem conditions on a seasonal to annual basis. An overview and description of the OTTER project is provided by Peterson and Waring (1993).

The Oregon test sites were selected on a west-to-east transect, along a temperature and moisture gradient that produces a large variation in ecosystem structure and function (Runyon et al., 1993). This transect, similar to that established by Gholz (1982), offers a very wide range of leaf area index values and crosses seven distinctive conifer vegetation zones. Each zone varies considerably in elevation and climate (Spanner et al., 1984). Conifer species composition of the vegetation zones is described in detail in Peterson et al. (1987). Canopy closure exceeds 75% for some of the western stands, and is as low as 15% for the eastern stands. The understory vegetation along the transect is composed of highly varying proportions of ferns, shrubs and grasses, with little exposed rock or soil (Spanner et al., 1990). Table 1 provides an overview of the sites.

There are two sites at Cascade Head—a closed canopy forest of mature conifers with virtually no understory, and a closed canopy of red alder with some understory. There are also two sites at Scio—an unfertilized site of closed canopy Douglas fir with virtually no understory, and a large fertilized stand with similar characteristics. Two sites are also found at Metolius

Table 1. Description of Test Sites

Name	Location	Dominant Species	Crown Closure
Juniper	Bend	Juniper	10–25%
Metolius River	East Cascades	Ponderosa / pine	25–50%
Waring's Woods	Corvalis	Douglas fir, oaks	>90%
Cascade Head	Coastal	Western hemlock, sitka spruce	100%
Scio	West Cascades	Douglas fir	100%

River. Both are open stands of ponderosa pine, recently cut over, with one site a control and the other being treated with nitrogen-rich sewage sludge. All of the other sites are large single stands of undisturbed forest. Only five sites were used in this study—Juniper, Scio fertilized, Metolius control, Waring's Woods, and Cascade Head.

Timber Measurements

The timber measurements were made in August 1991 at each of the five sites. At least 20 trees were selected at each stand for the measurement of height, crown width, DBH (diameter at breast height) and height-to-crown distance. The data were collected using variable-radius plot sampling. The general procedure was to lay out a transect through the stand using steel tape and hand-held compass and locate "points" along the transect. Each point is the center of a variable-radius plot (Dilworth, 1977). The points are separated by 30–50 m, depending on the size of the stand and the prism factor. The prism factor was selected in advance to require about four prism points to attain a sample of 20 trees.

The height, height-to-crown, and crown width were measured as follows. The height was obtained by clinometer for angle and steel tape for distance, while the crown width was measured using steel tape from below by looking up and judging when the tape indicates the edge of the crown. The DBH is measured with a diameter tape. In some stands (e.g., Juniper), trees with multiple stems were common; in that case, the DBHs of the multiple stems were measured, and then their basal areas were combined and reduced to a single DBH value to give the combined area. From the measurements, count density (trees/ha) was determined, and basal area weighted means of h, b, and r calculated.

SE-590 Radiometric Measurements

The geometric–optical model requires component signatures for calibration. These were collected using a Spectron Engineering SE-950 spectral radiometer. Since these component signatures will obviously vary according to time of day, the measurements were made whenever possible at a time close to the time of the ASAS overpass.

In collecting the radiance measurements, targets were selected to be representative of the types of surfaces within the ASAS field of view. Generally, targets were observed at zenith view angles of $+45°$, $0°$, and $-45°$ in the principal plane (here $+45°$ is taken as the direction near the hotspot peak). These angles were determined using a clinometer held against the case of the radiometer head. In the $+45°$ direction, it was often necessary to move away from the target in an azimuthal direction to avoid the shadow of the instrument and the operator. In general, measurements were made from 0.5 m to 1 m away from the target, and a single set of measurements was made for each target. During the measurement process, the first activity at a site was to record the radiance of a Spectralon panel. The clinometer was used to measure the solar zenith angle and the time of day was recorded. Then the radiances of the various cover types were measured, the scan number was recorded, and the cover type and viewing position were noted. Spectral measurements of sunlit and shaded crowns were difficult to make inside forest stands. In many cases, measurements were made on crowns at the edges of openings, where full-foliage branches were within reach. After the measurements were collected, the panel was measured once again, and the solar zenith angle and time of the day were also recorded.

The data normalization was carried out in two steps. First, the appropriate panel reference was established. Since the panel radiance varied between the start and end of the measurement period, a simple linear interpolation of the panel radiances was carried out between the first and last measurements. This established a separate panel reference for each measurement, which was then divided into the observed radiance. The second step was to adjust this reflectance to that of the Ames-2 SE-590 radiometer and the Ames-2 Spectralon panel using a set of calibration factors. These were standards agreed upon by the OTTER investigators. These calibration factors were calculated by ratioing the measurements of our panel by the Ames-2 radiometer with that made by the Ames-2 radiometer on the Ames-2 panel. A single calibration factor was calculated for every channel by combining these two ratios, and was later applied to the measured reflectance.

ASAS Imagery

The Advanced Solid-state Array Spectroradiometer (ASAS) is a pointable spectroradiometer with a unique capability to collect high spectral resolution data in the visible and near-infrared region of the spectrum at multiple directions (Irons et al., 1991). The ASAS detector is an area array providing 29 channels from 465 nm to 871 nm with an approximately 15 nm band width. Imagery from ASAS has a pixel size determined in the across-track direction by platform altitude, and in the along-track direction by the electronic readout rate and its 25° field of view. For the conditions of our acquisition, nadir pixel size was nominally 2.5 m × 4.0 m.

The ASAS instrument is currently operated by the NASA / Goddard Space Flight Center Laboratory of Terrestrial Physics and flown on NASA's C-130 aircraft. Data were collected during the period 19-21 June 1990; measurements were made for both high and low sun angles for all the sites under investigation. ASAS images were prepared and processed by the Terrestrial Physics Laboratory and were obtained from the Ames node of the Pilot Land Data System. Due to uncertainty and flight plans, it was not always possible to collect radiometric measurements concurrently with the overflights. Table 2 shows the correspondence between times and dates of collection.

Processing of the ASAS Images

Enhancement and Display

ASAS data were received in a format of two header records followed by 29 bands recorded in band-sequential format. The original 16-bit data were compressed to 8 bits as needed for image display, matching available software capabilities. Using three bands, 9 (556–570 nm), 16 (656–670 nm), and 21 (730–746 nm), coded as blue, green, and red, respectively, a color composite image was constructed for every scene. In order to give a better color image and still retain the different reflectance characteristics of each look angle, all images were stretched according to a histogram-normalized look-up table derived from the image closest to the hotspot position. Therefore, the images preserved their original brightness relative to each other.

Figures 2a–d show a set of the stretched images for four of the test sites. Seven images are shown, for each site beginning with the +45° image and ending with image at look angle −45°

Mean Radiance Calculation

For the model validation two ASAS bands, 16 (656–670 nm) and 25 (788–805 nm), were selected. These closely matched Channels 107 (RED) and 151 (NIR) of the SE-590 radiometer. For these bands, the mean radiance for each site at each look angle was calculated from 16-bit data. These mean radiance values were not calculated for the whole image, but, instead, for the specific stand where the ground radiometric measurements were made. The delineation of the stands in the ASAS images was aided by the use of color infrared airphotos. Figure 3 displays the mean radiance of the sites for the various look angles for Bands 16 and 25, together with a cross section through the principal plane of the modeled BRF.

Atmospheric Correction

For accurate and proper comparison between the model reflectance and the actual ASAS measured reflectance, the ASAS images were atmospherically corrected, thus allowing retrieval of the BRFs from the measured radiance, using a method developed by Liang and Strahler (1993).

The procedure of retrieving the BRFs from the ASAS data consisted of applying a series of models—a BRF model at the surface level; a radiative transfer atmospheric model at the atmosphere level; and a model for the measured radiance at the sensor level. With available information about any two models, the parameters of the third one can be retrieved. In this case, with the ASAS measured radiance at the sensor level and the atmospheric parameters available, the BRF values were retrieved. The BRF model is a statistical one consisting of six parameters. The atmospheric model uses a two-stream approximation and the atmospheric parameters of Rayleigh and aerosol optical depths as calculated from sunphotometer measurements that were collected approximately at the same times and dates of the ASAS overpass. An optimum algorithm was then applied to estimate the BRFs.

*Table 2.* Time Correspondence between ASAS and Ground Observation

Site	ASAS Overpass		Ground Observation	
	Date	Time	Date	Time
Juniper	19 Jun 90	16:17:05 GMT	19 Jun 90	15:50:00 GMT
Metolius River	19 Jun 90	16:37:00 GMT	19 Jun 90	17:50:00 GMT
Waring's Woods	19 Jun 90	19:39:10 GMT	21 Jun 90	16:50:00 GMT
Cascade Head	19 Jun 90	20:43:00 GMT	21 Jun 90	1:00:00 GMT
Scio	21 Jun 90	16:13:44 GMT	20 Jun 90	19:50:00 GMT

Figure 2. ASAS images of Juniper (a), Metolius (b), Waring's Woods (c), and Cascade Head (d) sites, showing the variations in brightness with the change in viewing angle. The top most is the +45° look angle and the bottom most is the −45°.

The two-stream approximation has been widely used before, unfortunately, one of assumptions associated with those researches is the Lambertian surface, which is not consistent in the present study. Liang and Strahler (1993) divide the radiation field into four components—unscattered radiance, single-scattering radiance, and two multiple-scattering radiances—and the last two components are calculated by the hybrid Eddington-delta approximation with some modifica-

tions. The original hybrid Eddington-delta formulae (Meador and Weaver, 1980) are from the nonreflective boundary condition; the new formulation can effectively take non-Lambertian surface into consideration. In order to retrieve BRF parameters effectively by means of an optimum algorithm, a simple statistical BRDF model is put forward based on the modified limacon model. This statistical BRDF model can capture angular features of the ground reflectance quite well. The Powell

(c)

(d)
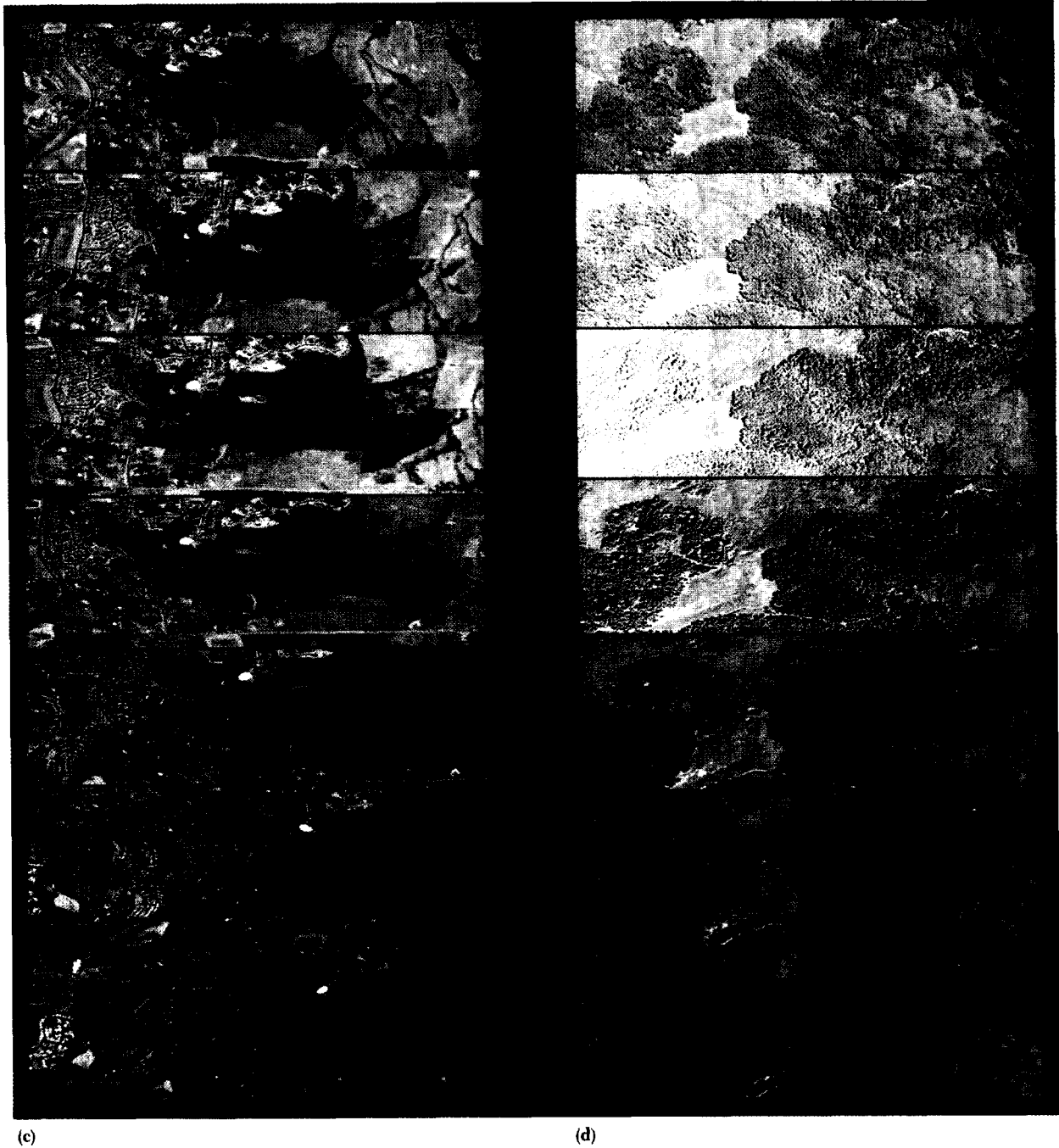
algorithm is used to search for the optimum estimates. Since the Powell algorithm does not require the explicit derivatives of the variables, we can deal with the complicated objective function, which combines the atmospheric model with the statistical BRDF model. Another significant feature of that inversion procedure is that we can retrieve not only BRF in the principal plane, but also the plane albedo even if only the radiance data in the principal plane are used. More details can be found in Liang and Strahler (1993).

BRF Calculation

The calculation of the BRF for each site using the mutual shadowing model required specifying a number of parameters, ranging from tree geometry to component signatures. In addition, the sun illumination angle and a value for β, calculated from the tree data according to (8), were also specified. Table 3 presents these parameters.

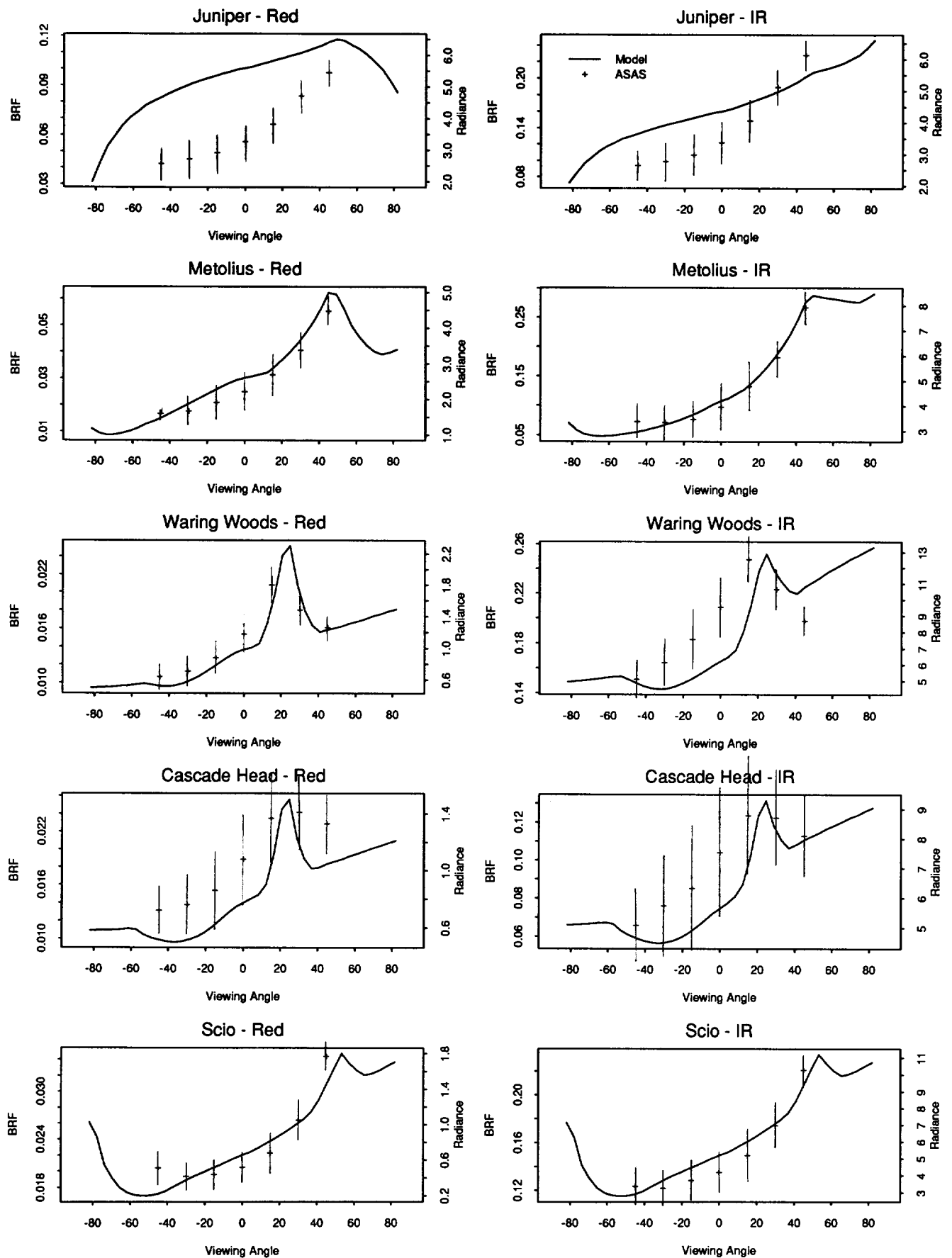Figures 4a and 4b display two sample BRFs, calculated for the Metolius site in red and near-infrared

Figure 3. Plots showing the variations in the ASAS radiance and model reflectance of the test sites with respect to changes in viewing angle.

Table 3. Parameters in BRF Calculation

Parameter	Juniper		Metolius River		Waring's Woods		Cascade Head		Scio	
	Red BRF	IR BRF	Red BRF	IR BRF	Red BRF	IR BRF	Red BRF	IR BRF	Red BRF	IR BRF
Density	50.050	50.500	876.500	876.500	333.000	333.000	393.750	393.750	1040.740	1040.750
Mean height	10.300	10.300	9.240	9.240	38.890	38.890	47.640	47.640	28.010	28.010
Height to crown	0.488	0.488	2.770	2.770	21.370	21.370	27.620	27.620	16.090	16.090
Crown width	5.610	5.610	2.880	2.880	6.650	6.650	6.096	6.096	5.000	5.000
G	0.132	0.188	0.132	0.188	0.059	0.135	0.059	0.135	0.059	0.135
C	0.077	0.270	0.044	0.319	0.021	0.286	0.023	0.139	0.035	0.238
Z	0.005	0.027	0.002	0.005	0.001	0.036	0.001	0.006	0.001	0.008
β	0.629	0.629	0.450	0.450	0.362	0.362	0.380	0.384	0.725	0.725
Sun angle	50.301	50.301	47.541	47.541	22.400	22.400	22.258	22.258	52.505	52.505

bands. In these plots, the BRFs are displayed in a cylindrical coordinate system. Each viewing position in the hemisphere is taken as a pair of polar coordinates, and the reflectance at that position is taken as the z-value. This produces a three-dimensional surface, which is then displayed as if viewed from behind. To allow comparison of the modeled reflectance and the ASAS reflectances, a cross-section line presenting the

modeled reflectance through the principal plane was extracted from each BRF plots for each site.

RESULTS AND DISCUSSION

The following discussion compares the BRF shape as captured by the ASAS in the mean radiance of Bands 16 and 25 with the Li–Strahler mutual shadowing model, which predicts the general shape of the BRF. In addition, the absolute magnitude of the BRFs of the model and the BRFs of the ASAS will be compared for Band 25.

Figure 3 presents plots of mean radiance values observed by ASAS in red and infrared, and the reflectance through the principal plane of the model for the five sites. For the Metolius and Scio sites, the shape of the modeled curves fit the ASAS radiance values fairly well. The hotspot peak, clearly shown in the model curves, is not apparent in the ASAS curves, because the sun angle at the time of the ASAS overpass (52° for Scio and 47° for Metolius) is greater than the maximum look angle of the ASAS at 45°, and is thus beyond its field of view, though the ASAS curves show a tendency toward higher reflectance at the hotspot image. The Juniper site does not fit the model well at all. Since this site has a low tree cover with abundant bare, reddish soil, the soil BRDF effects will be more important in determining the reflectance than the geometric optics of the tree layer. Further, this site was imaged at a high solar zenith angle with significant amounts of aerosol backscattering. Atmospheric correction (discussed below) reduced the IR variation to fit the modeled curve much more closely.

For the Waring's Woods and Cascade Head sites, the curves of the model and the ASAS show reasonable agreement. The observed hotspots seem broader than the modeled ones, although the hotspot position is shown more precisely in the model than by the ASAS values, as the aircraft images are restricted to a 15° increment.

The overall conclusion to be drawn from this analysis is that the ability of the model to predict the shape

Figure 4. Three-dimensional BRF plots for Metolius OTTER site in the red band (a) and infrared band (b).
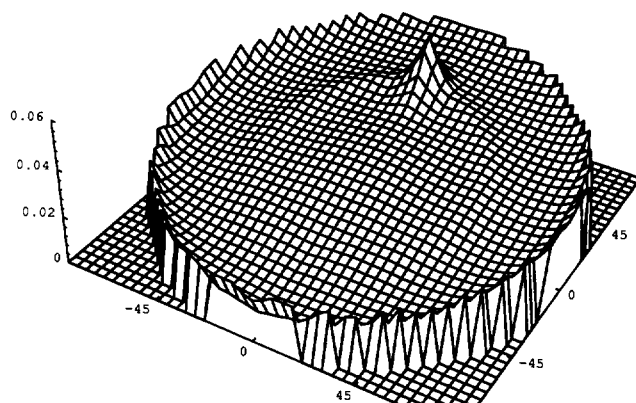
(a)
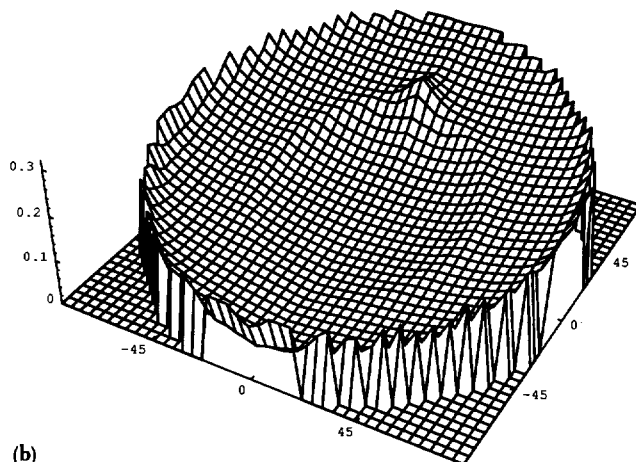
(b)

of the BRF is generally good. Encouraged by these results, we further attempted to validate the model by comparing its absolute BRF values to the ASAS BRF values atmospherically corrected by the Liang and Strahler (1993) method. These comparisons are only for the infrared (Band 25), however. This is because upon converting the ASAS brightness to units of radiance for the red band (16), the calculated radiances were far lower than the path radiances predicted by the atmospheric model. This anomalous result is most likely due to incorrect calibration of the ASAS detectors. Band 16, centered at 664 nm, is near the chlorophyll absorption maximum, and, consequently, the signal received by the ASAS in Band 16 is typically very low for vegetated targets. The ASAS detectors do not behave well at low signal levels due to low responsivity and what has been referred to as "build-up lag" (Irons, personal communication). These low light levels are below those available using existing calibration procedures, and consequently calibration factors may be inaccurate. For these reasons, our comparison is restricted to the infrared (Band 25).

Figures 5a–e display the cross section through the principal plane of the model BRFs and the ASAS BRFs. The match between the modeled and observed BRFs is best for the Juniper and Metolius sites. At Metolius, the shapes are quite close, but the overall observed reflectance level is brighter than the modeled. At the Juniper site, the magnitude is very close, but the model predicts a flatter slope for the BRF. This occurs because the component signatures are simply subjected to a cosine correction with angle, and since the canopy cover is so low, the sunlit background dominates. Presumably, the true response of the soil at the Juniper site departs from this Lambertian assumption.

In the Cascade Head and Waring's Woods sites, the model tends to underestimate the scene BRFs. For these sites, the time of the ground SE-590 observations of component signatures and the ASAS overpass did not coincide because some of the ASAS overflights were cancelled or obtained data of poor quality. This appears to have strongly affected the modeled BRFs. While the ASAS overpass over Cascade Head was early in the day (sun angle 22°), the SE-590 ground measurements were made late in the day (sun angle 68°); thus the component signatures used to calculate the BRFs are probably darker than the actual ones measured by the ASAS. Had the two measurements coincided in observation timing, better results may have been displayed. The lack of coincidence in time between ground and aircraft overpass is also believed to have affected the modeled BRFs of the Waring's Woods site. Here the SE-590 observations were made in the midmorning (sun angle 38°), while the ASAS overpass was early afternoon (sun angle 22°). Thus, the ASAS measurements are brighter than those predicted by the SE-590 component signatures.

In an attempt to enhance the fit and rectify the problem of darker signatures, we assumed that the component signatures varied simply as the cosine of the sun angle at the time of the two measurements. This boosted Cascade Head BRFs approximately 55%, thus reducing the discrepancy in the magnitude of the BRFs. Similarly the signatures at Waring's Woods were increased by 13%, to display better results. Although the improvement is in the right direction, it appears that a simple cosine correction does not boost the signal sufficiently. This may be due to nonlinearity of the multiple scattering component, which will be strong in the near infrared.

The results from the model for the Scio site are different than the other ones. This is the most dense site of all the five, with nearly 100% crown closure and a different canopy structure. In the figure, the ASAS images show higher BRFs than those of the model; as at Waring's Woods and Cascade Head, there was a significant difference in the timing of the ASAS overpass and the acquisition of component signatures. Another problem relates to measurement of the sunlit crown component signature. In dense stands where the trees are spaced very closely, the model assumes that the major portion of the area is in sunlit crown. For the Scio site, sunlit crown signatures were collected from lower branches of trees exposed to full sunlight at the edge of the stand. A signature obtained from the top of the tree looking into the canopy would be expected to be significantly brighter, due to multiple scattering in the infrared.

In general, the modeled hotspots tend to be narrower than those observed for the ASAS data. A possible reason for this lies in the measurement of the component signatures. It is likely that the brightness contrast among sunlit crown, shaded crown, and shaded background is enhanced by the measurement technique, which, in turn, would accentuate the sharpness of the hotspot. Shaded crown measurements, like those of sunlit crown, were made on lower branches of trees in sunlit and shaded conditions. However, the shaded crown seen by the ASAS is much nearer the top of the canopy, where it is likely to be brighter. Further, shaded background measurements were often made under the tree canopy, whereas the shaded background viewed by the ASAS would be background in shade under an opening in the canopy. Under these conditions, the shaded background component signatures are probably darker than they should be. It is notable that the best fit shapes are from the Metolius and Juniper sites, where the stands are quite open and the trees are small. Under these conditions component signatures are easier to measure more accurately.

CONCLUSIONS

Because many natural vegetation covers may be regarded as assemblages of plant crowns that are located on a background plane and interact with light as discrete
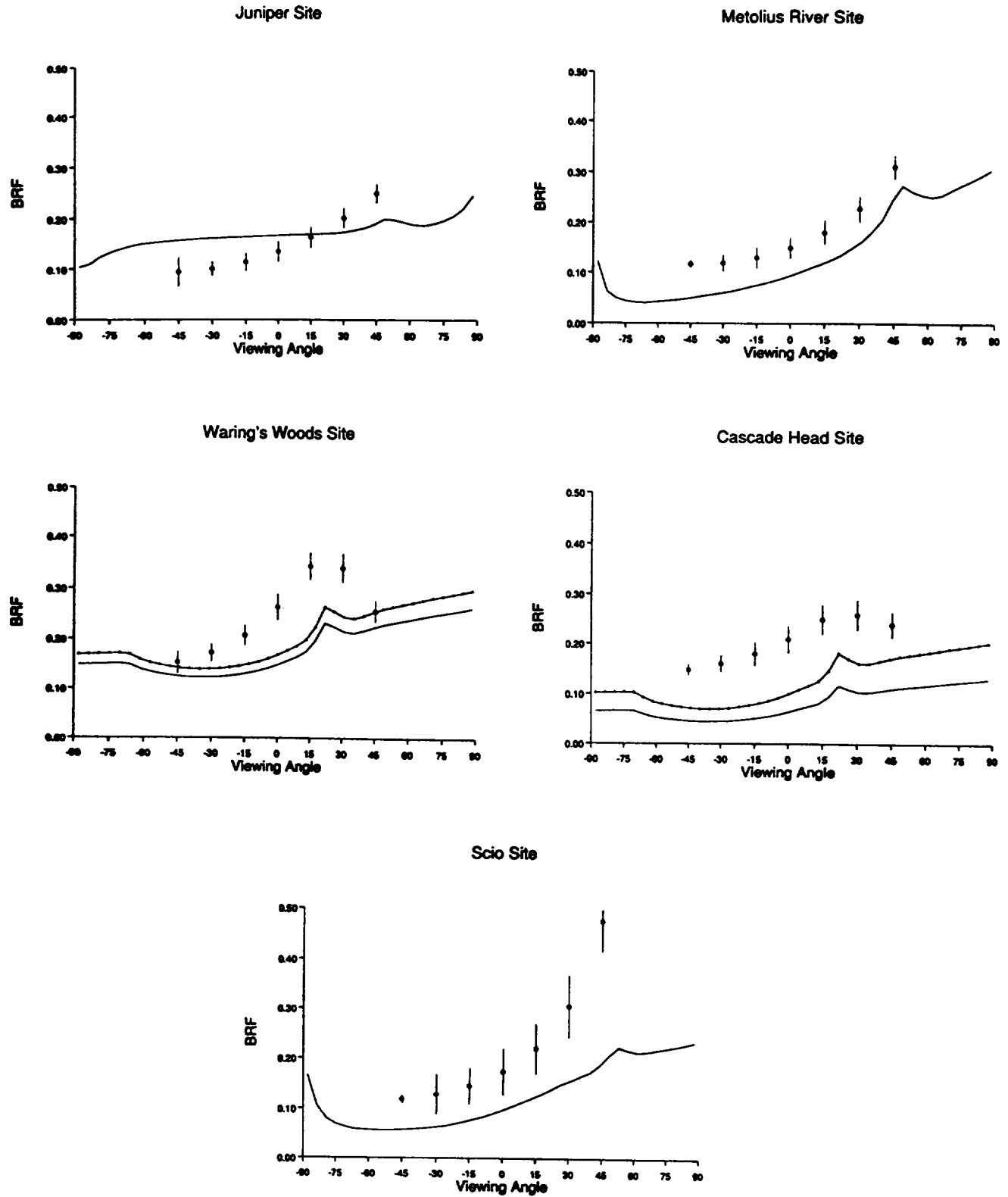
Figure 5. Cross-sectional plots of the OTTER sites BRFs as calculated by the model and measured by the ASAS.

objects, geometric optics can provide an approach to model the bidirectional distribution function of natural vegetation canopies that captures the most important features exhibited by bidirectional measurements of such canopies. The Li-Strahler geometric–optical model utilized here exploits the primary mechanism of three-dimensional shadowing that relates size, shape, and count density of plant crowns to viewing and illumination positions and crown-background reflectance contrasts. From our validation studies here, the model seems to work well when component signatures are properly acquired to calibrate it.

Our validation exercise suggest a number of ways in which our model and associated techniques can be improved. The most significant is the improvement of the measurement technique for component signatures. Because of the difficulty in obtaining radiometer measurements of sunlit and shaded tree canopy from above, measurements taken from trees at the edge of the stand under direct solar illumination were used. These are most likely different—probably lighter in the red and darker in the infrared—than measurements acquired from the viewpoint of an airborne or spaceborne sensor. Further, shaded background signatures should be acquired in small clearings or patches open to the sky above. Also, greater effort should be taken to ensure that measurements coincide closely in time with the sensor overpass.

The Li–Strahler model is formulated under the assumption that tree crowns are opaque, and thus shadowed signatures are uniformly dark. This is unrealistic for real canopies; light may pass directly through a tree crown in gaps between branches and leaves, and, further, leaves have transmittance and therefore radiation passes through leaves. Also, the model does not account for the multiple scattering between crowns and the ground. Although these deficiencies are somewhat alleviated by using component signatures that include multiple scattering, gaps, and transmittance, it may prove possible to accommodate these effects, as well as improvements in the radiometric measurement techniques, to improve the accuracy and performance of the model.

The fact that the Li–Strahler model captures the basic features of the variance in directional reflectance for the OTTER forest stands leads to speculation on the possibility of inversion to yield remote estimates of plant size, shape, and count density from angular radiance measurements. Although a full discussion of the inversion problem is beyond the scope of this article, we should note that inversion of the Li–Strahler model for the nadir-viewed case using Landsat Thematic Mapper data has provided reasonable estimates of tree height and density for similar Oregon conifer stands (Wu and Strahler, 1993). That inversion uses spatial variance, whereas the approach of this article is to model angular variance. However, with a full characterization of spatial variance, angular variance, and the relation between the two induced by the nature of the objects in the scene and their illumintion conditions (Jupp et al., 1991), a complex, but probably quite accurate, inversion procedure might be derived.

REFERENCES

Chandrasekhar, S. (1950), *Radiative Transfer*, Oxford University Press, London.

Cooper, K., Smith, J. A., and Pitts, D. (1982), Reflectance of a vegetation canopy using the adding method, *Appl. Opt.* 21:4112–4118.

Dilworth, J. (1977), *Log Scaling and Timber Cruising*, OSU Book Stores, Corvalis, OR.

Gerstl, S. A. W., Simmer, A. C., and Powers, B. J. (1986), The canopy hot-spot as crop identifier, in *Symposium on Remote Sensing for Resources Development and Environmental Management*, Enschede, August, pp. 261–263.

Gholz, H. L. (1982), Environmental limits on aboveground net primary production, leaf area, and biomass in vegetation zones of the Pacific Northwest, *Ecology* 63(2):469–481.

Irons, J. R., Ranson, K. J., Williams, D. L., Irish, R. R., and Huegel, F. G. (1991), An off-nadir pointing imaging spectroradiometer for terrestrial ecosystem studies, *IEEE Trans. Geosci. Remote Sens.* 29:66–74.

Jackson, R. D., Reginato, R. J., Pinter, P. J., Jr., and Idso, S. B. (1979), Plant canopy information extraction from composite scene reflectance or row crops, *Appl. Opt.* 18: 3775–3781.

Jupp, D. L. B., and Strahler, A. H. (1991), A hotspot model for leaf canopies, *Remote Sens. Environ.* 38:193–210.

Jupp, D. L. B., Walker, J., and Penridge, L. K. (1986), Interpretation of vegetation structure in Landsat MSS imagery: a case study in distributed semiarid eucalypt woodlands, Part 2: Model-based analysis, *J. Environ. Manage.* 23:35–57.

Jupp, D. L. B., Walker, J., Harrison, B., Strahler, A. H., and Li, X. (1991), Using local spatial variance and directional radiance to monitor the structure of woodlands and forests, in *Proceedings of the 12th Asian Conference on Remote Sensing*, SEAMEO, Singapore, 30 October–5 November, 8 pp.

Kimes, D. S. (1984), Modeling the directional reflectance from complete homogeneous vegetation canopies with various leaf-orientation distributions, *J. Opt. Soc. Am.* 1(7):725–737.

Kimes, D. S., Newcomb, W. W., Nelson, R. F., and Schutt, J. B. (1986), Directional reflectance distributions of a hardwood and a pine forest canopy, *IEEE Trans. Geosci. Remote Sens.* 24:281–293.

Kubelka, P., and Monk, F. (1931), Ein Beitrag zur Optik der Farbanstruck, *Z. Tech. Phys.* 11:593–601.

Kuusk, A. (1985), The hot spot effect of a uniform vegetation cover, *Sov. J. Remote Sen.* 3(4):645–658 (Engl. transl.).

Li, X., and Strahler, A. H. (1985), Geometric optical modeling of a conifer forest canopy, *IEEE Trans. Geosci. Remote Sens.* 23:207–221.

Li, X., and Strahler, A. H. (1986), Geometric-Optical bidirectional reflectance modeling of a conifer forest canopy, *IEEE Trans. Geosci. Remote Sens.* 24:906–919.

Li, X., and Strahler, A. H. (1992a), Geometric optical bidirectional reflectance modeling of the discrete crown vegetation canopy: effect of crown shape and mutual shadowing, *IEEE Trans. Geosci. Remote Sens.* 30:276–292.

Li, X., and Strahler, A. H. (1992b). Mutual shadowing and directional reflectance of a rough surface: a geometric-optical model, in *Proceedings, IGARSS '92*, 26–29 May, Houston, TX, pp. 766–768.

Liang, S., and Strahler, A. H. (1993), Retrieval of surface BRDF and albedo from multiangle remotely sensed data, forthcoming.

Marshak, A. L. (1989), The effect of the hot spot on the transport equation in plant canopies, *Quant. Spectrosc. Radiat. Transfer* 42:615–630.

Meador, W.E., and Weaver, W.R. (1980), Two-stream approximations to radiative transfer in planetary atmospheres: a unified description of existing methods and a new improvement, *J. Atmos. Sci.* 37:630–643.

Myneni, R. B., and Ross, J., Eds. (1991), *Photon–Vegetation Interactions*, Springer-Verlag, Berlin.

Myneni, R.B., Asrar, G., and Gerstl, S. A. W. (1990), Radiative transfer in three dimensional leaf canopies, *Transport Theory Stat. Phys.* 19:205–250.

Myneni, R. B., Marshak, A., Knyazikhin, Y., and Asrar, G. (1991), Discrete ordinates method for photon transport in leaf canopies, in *Photon–Vegetation Interactions* (R. B. Myneni and J. Ross, Eds.), Springer-Verlag, Berlin, pp. 45–109.

Nilson, T. (1977), A theory of radiation penetration into non-homogeneous plant canopies. In *The Penetration of Solar Radiation into Plant Canopies*, Tartu Acad. Sci. ESSR: 5–70 (in Russian).

Nilson, T., and Kuusk, A. (1989), A reflectance model for the homogeneous plant canopy and its inversion, *Remote Sens. Environ.* 27:157–167.

Nilson, T., and Peterson, U. (1991), A forest canopy reflectance model and test case, *Remote Sens. Environ.* 37:131–142.

Otterman, J., and Weiss, G. H. (1984), Reflection from a field of randomly located vertical protrusions, *Appl. Opt.* 23:1931–1936.

Peterson, D. L., and Waring, R. H. (1993), Overview of the Oregon Transect Ecosystem Research Project, *Ecol. Appl.*, forthcoming.

Peterson, D. L., Spanner, M. A., Running, S. W., and Teuber, K. B. (1987), Relationship of Thematic Mapper Simulator data to leaf area index of temperate coniferous forest, *Remote Sens. Environ.* 22:323–341.

Reyna, E., and Bhadwar, G. D. (1985), Inclusion of specular reflectance in vegetative canopy models, *IEEE Trans. Geosci. Remote Sens.* 23:731–736.

Ross, J. (1981), *The Radiation Regime and Architecture of Plant Stands*, Dr. W. Junk, The Hague.

Runyon, J., Waring, R. H., Goward, S. N., and Welles, J. M. (1993), Environmental limits on above-ground production: observations from the Oregon Transect, *Ecol. Appl.* forthcoming.

Serra, J. (1982), *Image Analysis and Mathematical Morphology*, Academic, London and New York.

Spanner, M. A., Peterson, D. L., Hall, M. J., Wrigley, R. C., Card, D. H., and Running, S. W. (1984), Atmospheric effect on the remote sensing estimation of forest leaf area index, in *Proceedings of the Eighteenth International Symposium on Remote Sensing of Environment*, Paris, pp. 1295–1308.

Spanner, M. A., Pierce, L. L., Peterson, D. L., and Running, S. W. (1990), Remote sensing of coniferous forest leaf area index. The influence of canopy closure, understory vegetation and background reflectance, *Int. J. Remote Sens.* 11:95–111.

Strahler, A. H., and Jupp, D. L. (1990), Modeling bidirectional reflectance of forests and woodlands using Boolean models and geometric optics. *Remote Sens. Environ.* 34:153–166.

Suits, G. H. (1972a), The calculation of the directional reflectance of a vegetation canopy, *Remote Sens. Environ.* 2:117–125.

Suits, G. H. (1972b), The cause of azimuthal variations in directional reflectance, *Remote Sens. Environ.* 2:175–182.

Verhoef, W. (1984), Light scattering by leaf layers with application to canopy reflectance modeling: the SAIL model, *Remote Sens. Environ.* 16:125–141.

Verstraete, M. M., Pinty, B., and Dickson, R. E. (1990), A physical model of the bidirectional reflectance of vegetation canopies: I. Theory, *J. Geophys. Res.* 95:11,755–11,765.

Wu, Y., and Strahler, A. H. (1993), Remote estimation of crown size, stand density, and biomass on the Oregon Transect, *Ecol. Appl.*, forthcoming.